Journal of Electronic Materials (2022) 51:3579–3588
https://doi.org/10.1007/s11664-022-09599-3

ORIGINAL RESEARCH ARTICLE

Improved β-Ga_2O_3 Solar-Blind Deep-Ultraviolet Thin-Film Transistor Based on Si-Doping

Leyun Shen[1] · **Xinhua Pan**[1,2] · **Tao Zhang**[1] · **Yunze Liu**[1] · **Ning Wang**[1] · **Peng Wang**[1] · **Fengzhi Wang**[1,2] · **Guangmin Zhu**[3] · **Jiangbo Wang**[3] · **Zhizhen Ye**[1,2]

Received: 10 February 2022 / Accepted: 21 March 2022 / Published online: 13 April 2022
© The Minerals, Metals & Materials Society 2022

Abstract

Gallium oxide (Ga_2O_3)-based photodetectors are attracting more and more attention for their wide range of applications in optical imaging, spatial communication, etc. In this work, solar-blind deep-ultraviolet thin-film transistors (TFTs) based on polycrystalline β-Ga_2O_3 thin film were constructed by pulsed laser deposition. The photoelectric performance of β-Ga_2O_3 TFT is effectively improved by a Si-doping method. The turn-on voltage (V_{on}) of Si-doped β-Ga_2O_3 TFT is negatively shifted by 20 V, exhibiting enhancement-mode (E-mode) operation. The optimized Si-doped Ga_2O_3 TFT photodetector shows a high on/off ratio of ~ 10^5, a turn-off current (I_{off}) of ~ 10^{-11} A at drain voltage (V_D) = + 20 V, responsivity (R) of 3.23 A/W, detectivity (D^*) of 4.41 × 10^{13} Jones, and a photocurrent/dark current (I_{light}/I_{dark}) of ~ 10^4 at gate voltage (V_G) = − 5 V, V_D = + 20 V under 254 nm light. The obtained results suggest that the Si-doping method can effectively modulate the V_{on} of β-Ga_2O_3 TFT and promote photoelectric performance.

Keywords Ga_2O_3 · Si-doping · photodetectors · thin-film transistor · pulsed laser deposition

Introduction

Recently, β-phase gallium oxide (β-Ga_2O_3) has achieved great attention as a promising semiconductor material for high-power electronics. Ga_2O_3, with an ultra-large energy band gap of ~ 4.8 eV, is of great potential in deep-ultraviolet (DUV) detection.[1] DUV signatures have a weak solar background interface because of strong absorption of stratospheric ozone, contributing to applications in flame detection, missile early alarm, and so on.[2] Therefore, photodetectors based on β-Ga_2O_3 have been widely studied in recent years.[3–6] Furthermore, the Baliga's figure of β-Ga_2O_3 at 3214 is considerably higher than those of SiC at 317 and GaN at 846,[7] which means that β-Ga_2O_3 electronics are more efficient than other wide band-gap materials.

β-Ga_2O_3 photodetectors have been developed rapidly based on various structures, such as Schottky barriers,[5,6] p–n junctions,[8–10] metal–semiconductor–metal (MSM),[11,12] etc. Recently, Ga_2O_3 -based thin-film transistors (TFT) have received increasing attention and been successfully demonstrated.[13–18] TFT-type devices achieve excellent photoelectric performance through three-terminal control, and easily integrate with other devices in circuits.[19] Most transistors are based on bulk single-crystal β-Ga_2O_3. Jinho et al. demonstrated a dual-field single-crystal β-Ga_2O_3 nano-field effect transistor (FET) with an off-state hard breakdown voltage exceeding + 400 V.[15] Yaxuan et al. obtained FET solar-blind photodetectors based on high-quality single-crystalline Ga_2O_3 flakes, achieving high photocurrent/dark current (I_{light}/I_{dark}) of 8 × 10^5, a responsivity (R) of 4.79 × 10^5 A/W, and an external quantum efficiency (EQE) of 2.34 × 10^6%.[18] However, high-quality materials always demand strict experimental conditions. Differently, β-Ga_2O_3 thin films make up for the defects of bulk materials, along with low cost, easy growth, great repeatability and flexibility,[3,10,11]

✉ Xinhua Pan
panxinhua@zju.edu.cn

[1] State Key Laboratory of Silicon Materials, School of Materials Science and Engineering, Zhejiang University, Hangzhou 310027, People's Republic of China

[2] Wenzhou Key Laboratory of Novel Optoelectronic and Nano Materials, Institute of Wenzhou, Zhejiang University, Wenzhou 325006, People's Republic of China

[3] Key Laboratory of Wide Bandgap Semiconductor Materials and Devices, Yiwu 322009, Zhejiang, People's Republic of China

most of which show polycrystalline or amorphous phrases prepared by pulsed laser deposition (PLD), metal–organic chemical vapor deposition (MOCVD), sputtering, and spin-coating. Yuan et al. pioneered an enhancement-mode solar-blind metal-oxide–semiconductor field-effect phototransistor based on molecular beam epitaxy (MBE) homoepitaxial β-Ga_2O_3 film, obtaining a high *R* of 3×10^3 A/W, an EQE of 1.5×10^6%, and short rise and decay times of 100 ms and 30 ms,[17] respectively. Xi et al. presented amorphous Ga_2O_3:CdO thin film-based TFT devices prepared by spin-coating, and demonstrated a large negative shift in the turn-on voltage (V_{on}) due to the increase in the electron concentration.[14] Yuan et al. investigated a solar-blind phototransistor based on low-cost magnetron-sputtered amorphous GaO_x thin film, which achieved ultra-high responsivity, detectivity (D^*), and EQE.[16]

Here, we demonstrate polycrystalline β-Ga_2O_3 solar-blind DUV TFTs with gate-tunable photodetection. PLD was used to deposit the β-Ga_2O_3 thin film on a Si/SiO_2 substrate to fabricate TFT-type devices. We discuss the characteristics of the deposited β-Ga_2O_3 thin film with and without Si-doping, including their crystallinity, morphology, and defects. Moreover, the electric and photoresponse performances of TFTs based on pure β-Ga_2O_3 and Si-doped β-Ga_2O_3 are analyzed.

Experimental

β-Ga_2O_3 Preparation and Device Fabrication

A *p*-type Si substrate was cleaned in acetone, alcohol, and deionized water. PLD was used to deposit the β-Ga_2O_3 thin film on the (100)-oriented Si with a 320-nm SiO_2 layer. A highly purified (99.99%) Ga_2O_3 ceramic target and a Si-doped Ga_2O_3 ceramic target (Ga_2O_3: SiO_2 = 99.5: 0.5 wt%) were used, respectively, both of which were 50.8 mm in diameter and 5 mm in thickness. The target–substrate distance was 69 mm. The substrate temperature during deposition was fixed at 700 °C. The deposition chamber was pumped down to a base pressure of 3×10^{-5} Pa. Subsequently, a working pressure of oxygen of 0.1 Pa was introduced. A 248-nm KrF excimer laser, with a repetition rate of 3 Hz and an energy density of 5 J cm^{-2} , was used to deposit β-Ga_2O_3 thin films for 30 min. Next, the Ga_2O_3 thin films were annealed at 800 °C by a rapid thermal annealing method for 30 min, reducing defects such as oxygen vacancies.[20] To fabricate the TFT, Si wafers with a SiO_2 layer were used as the gate electrode, gate dielectric, and substrates. The drain/source electrode regions were defined by depositing Au/Ti (50/20 nm) using e-beam evaporation through a shadow mask. The length and width of the channel were 1000 µm and 100 µm, respectively.

Material and Device Characterization

X-ray diffraction (XRD; PANalytical X-pert Powder) with CuKα radiation was used to measure the crystalline properties of the films. The surface morphologies and roughnesses of the films were characterized by scanning electron microscopy (SEM; SU-70; Hitachi) and atomic force microscopy (AFM; Multimode-8; Bruker Nano). The defect type and content were examined by x-ray photoelectron spectroscopy (XPS; Kratos AXIS Supra). The electrical performance was measured using semiconductor parameter analyzers (Keithley 4200). A 254-nm ultraviolet (UV) light-emitting diode was provided as the light source to measure the photoresponse properties.

Results and Discussion

The XRD study was carried out on pure β-Ga_2O_3 film and Si-doped β-Ga_2O_3 film. Figure 1a shows the XRD diffraction patterns of the Ga_2O_3 films grown on the (100) Si substrate deposited at 700 °C. Both samples show polycrystalline β-Ga_2O_3 with a monoclinic structure. The peaks indexed to (− 201), (110), (− 402) and (− 601) are dominant in the pure β-Ga_2O_3 film, while such peaks decrease in the Si-doped β-Ga_2O_3 film, indicating that the Si-doping method might have reduced the crystallinity in the presence of lattice distortion. Different growth temperatures and the rapid thermal annealing method are also discussed in detail in the Supporting Information (see Figures S1, S2). A cross-section SEM image of β-Ga_2O_3 is shown in Fig. 1b. The thickness of the β-Ga_2O_3 film is ~ 86 nm (depositing time 30 min). Figure 1c and d present the 3D AFM images of the surface of the β-Ga_2O_3 films in a 5×5 µm^2 area. The root-mean-square surface roughness of the Si-doped β-Ga_2O_3 films is 1.26 nm, which is smaller than that of pure β-Ga_2O_3 films (2.59 nm), suggesting that the Si-doped β-Ga_2O_3 film is relatively smooth. Pure Ga_2O_3 film exhibits a state of high resistance while the carrier density is 9.5×10^{10} cm^{-3}. The Si-doped Ga_2O_3 film exhibits *n*-type conductance, and the resistivity and carrier density are 1986 Ω cm and 2.4×10^{16} cm^{-3}, respectively, as previously reported.[21] In brief, the crystal quality is slightly reduced after Si-doping, and both films are of good quality with flat surfaces and high uniformity.

XPS measurements were performed to identify defect types and defect concentrations. The charge–shift spectrum was calibrated using an adventitious C 1*s* peak at 284.8 eV. Figure 2a and d shows the XPS survey scan of pure β-Ga_2O_3 thin film and Si-doped β-Ga_2O_3 thin film, respectively. Both curves show characteristic peaks of Ga

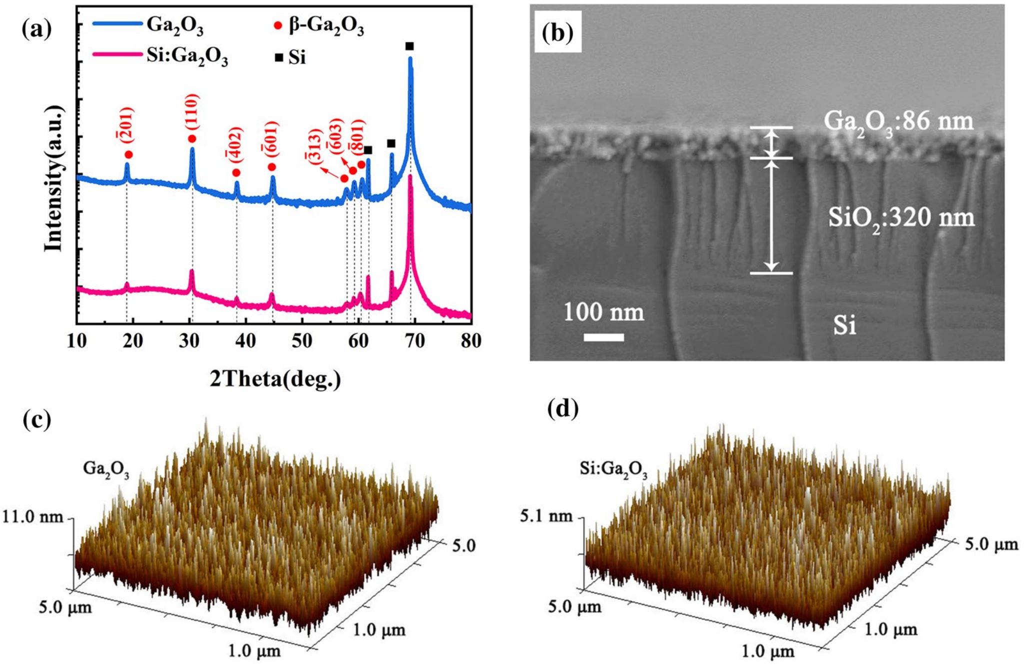

Fig. 1 (a) XRD curves of pure β-Ga_2O_3 film and Si-doped β-Ga_2O_3 film. (b) Cross-section SEM image of β-Ga_2O_3 film. AFM images of (c) pure β-Ga_2O_3 film and (d) Si-doped β-Ga_2O_3 film.

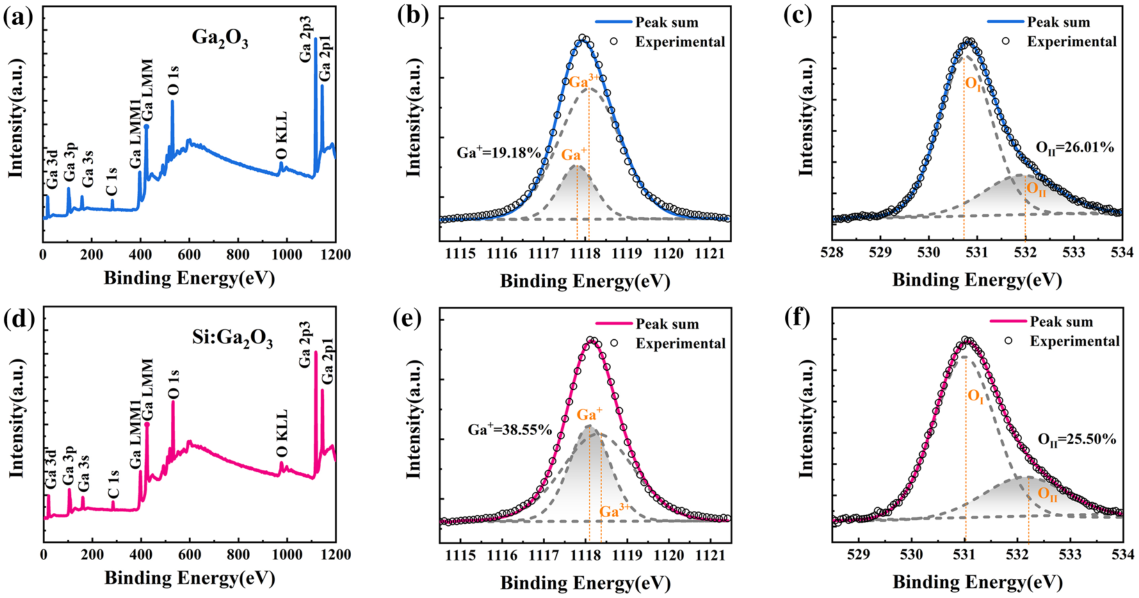

Fig. 2 (a) XPS spectra of pure β-Ga_2O_3 thin film. (b, c) Ga 2*p* core peak and O 1*s* peak of pure β-Ga_2O_3 thin film, respectively. (d) XPS spectra of Si-doped β-Ga_2O_3 thin film. (e, f) Ga 2*p* core peak and O 1*s* peak of Si-doped β-Ga_2O_3 thin film, respectively.

(2*p*, 3*p*, 3*d*), O (1*s*) and C (1*s*), and there is no significant difference between them. Thus, a small amount of Si-doping would not have a huge impact on the composition of thin films. Recent studies show that Si would diffuse into the oxide from the Si substrate when annealed at a higher temperature.[22,23] Similar situations have occurred in Al_2O_3, GaN, and so on.[24,25] The XPS narrow scans of the Ga 2*p* core level and O 1*s* level were also conducted. Figure 2b and e shows the Ga 2*p* peaks of pure Ga_2O_3 film and Si-doped Ga_2O_3 film, respectively. The Ga 2*p* peak can be separated into two peaks, one corresponding to Ga^+ (Ga_2O), the other to Ga^{3+} $(Ga_2O_3)^4$. For pure Ga_2O_3, the relatively lower peak appears at 1117.8 eV (Ga^+), and its higher peak appears at 1118.1 eV (Ga^{3+}). The peak ratio of Ga^+/Ga^{3+} is 19.18%. For the Si-doped Ga_2O_3, the peak ratio increases to 38.55%, implying that the Ga_2O_3 content reduces and crystal quality degrades. In other words, Si-doping results in poor crystallization, which might be caused by lattice distortion and changed electron orbits. Therefore, the XPS results exactly match with the XRD curves (see Fig. 1a). From Fig. 2c and f, the O 1*s* peaks of two samples are compared and the charge–shift can be divided into two components: the lower one is assigned to lattice oxygen ions (O_I), and the other to the oxygen ions in the oxygen vacancies regions (O_{II}).[26–28] Thus, the peak ratio of O_{II}/ O_I is used to characterize the content of the oxygen vacancies, while there is little difference between the two samples, 26.01% and 25.50%, for pure Ga_2O_3 and Si-doped Ga_2O_3 , respectively. It is said that there is no obvious relevance between oxygen vacancies and Si-doping. It is worth noting that the binding energy (BE) of Si-doped samples positively shifts by 0.2–0.3 eV. Since the Si atoms are expected to be the electron donor, the carrier concentration increases correspondingly, resulting in Fermi-level movement. Absorption curves show a lower band gap of the Si-doped sample compared to the pure one (see Figure S3, Supporting Information). Therefore, the BE peaks shift to being higher because of Fermi-level movement (for the details of the XPS analysis data, see Table SI in Supporting Information).[23]

The bottom-gate TFTs were fabricated employing those β-Ga_2O_3 thin films as channels, and the device's schematic structure is shown in Fig. 3a. To explore the photoelectric characteristics of β-Ga_2O_3 TFT, optoelectronic performance measurements were conducted under 254-nm DUV light illumination with an intensity of 245.9 $\mu W\ cm^{-2}$. Figure 3b presents the drain current (I_D)-gate voltage (V_G) transfer curves of pure β-Ga_2O_3 and Si-doped Ga_2O_3 TFTs in the dark and under illumination. Over the channel current, the gate shows an apparent field-effect control ability and a low turn-off current (I_{off}) of ~ 10^{-11} A. The on/off ratio of pure β-Ga_2O_3 TFT is over 10^5 at the drain voltage (V_D) = + 20 V, and there is a slight increase in the on/off ratio after Si-doping. Furthermore, Si-doped Ga_2O_3 TFT shows a V_{on} of − 4.4 V, while the V_{on} of pure β-Ga_2O_3 TFT is 14.3 V. That is to say, the Si-doped Ga_2O_3 TFT works in depletion mode and the pure β-Ga_2O_3 TFT works in enhancement mode. A negative shift of V_{on} (about − 20 V) is observed in the Si-doped sample. β-Ga_2O_3 prepared by PLD has a high resistance due to the many oxygen vacancies and other defects,[29] so it is inevitable that the V_{on} of the device is large. It is said that pure Ga_2O_3 TFT is usually turned on with difficulty. For more carriers supplied by Si-doped TFT, it is easier to present an open state when it reaches a certain value. In addition, the estimated field-effect carrier mobility (μ_{FE}) of the pure and Si-doped samples are 0.14 $cm^2\ V^{-1}\ s^{-1}$ and 0.15 $cm^2\ V^{-1}\ s^{-1}$, respectively, verifying the effect of increasing carrier concentration on mobility. The μ_{FE} can be obtained from the following:[30]

$$\mu_{\mathrm{FE}} = \frac{L}{W}\frac{2}{C_{\mathrm{g}}}\left(\frac{\partial\sqrt{I_{\mathrm{D}}}}{\partial V_{\mathrm{G}}}\right)^2, \tag{1}$$

where *L* and *W* denote the length and width of the channel, respectively, C_g is the gate dielectric capacitance per unit area, and V_G is the gate bias. Similarly, the photocurrent of the Si-doped Ga_2O_3 TFT is larger than that of pure Ga_2O_3 TFT due to a higher carrier concentration. The measured results demonstrate that the I_{light}/I_{dark} is higher than 10^4, showing ultra-high sensitivity under DUV light. In order to quantitatively assess the photoelectric performance of both Ga_2O_3 TFTs, key figure-of-merit of the photodetectors have been calculated. The responsivity is defined as the photocurrent generated per unit power of the incident light on the effective area of a photodetector, which can be obtained at $V_D = +\ 20$ V bias as follows:

$$R = \frac{I_{\mathrm{light}} - I_{\mathrm{dark}}}{P_{\lambda}S}, \tag{2}$$

where I_{light} is the photocurrent, I_{dark} is the dark current, P_λ is the light intensity, and *S* is the effective illumination area of the device. As shown in Fig. 3b, the *R* of the pure Ga_2O_3 TFT and the Si-doped Ga_2O_3 TFT are estimated to be 2.20 A/W ($V_G = +\ 5$ V) and 3.23 A/W ($V_G = -\ 5$ V), respectively, indicating the sensitivity of β-Ga_2O_3 photodetectors in the solar-blind region. The EQE factor can be determined by:

$$\mathrm{EQE} = \frac{hc}{q\lambda}R \times 10^2\%, \tag{3}$$

where *h* is the Plank's constant, *c* is the velocity of light, and *λ* is the wavelength of light. The EQE of the pure Ga_2O_3 TFT and the Si-doped Ga_2O_3 TFT are estimated to be $1.1 \times 10^3\%$ and $1.6 \times 10^3\%$, respectively, under corresponding conditions. Another important factor, D^* , which is usually used to describe the smallest detectable signal, can be expressed by:

$$D^* = \frac{RS^{1/2}}{\left(2qI_{\mathrm{dark}}\right)^{1/2}}. \tag{4}$$

The D^* of the pure and Si-doped samples are calculated to be as high as 4.23×10^{13} Jones and 4.41×10^{13} Jones, respectively, surpassing most ever-reported Ga_2O_3 photodetectors.[9,14,31] The high D^* can offset the impact of the noise from the relatively high dark current.

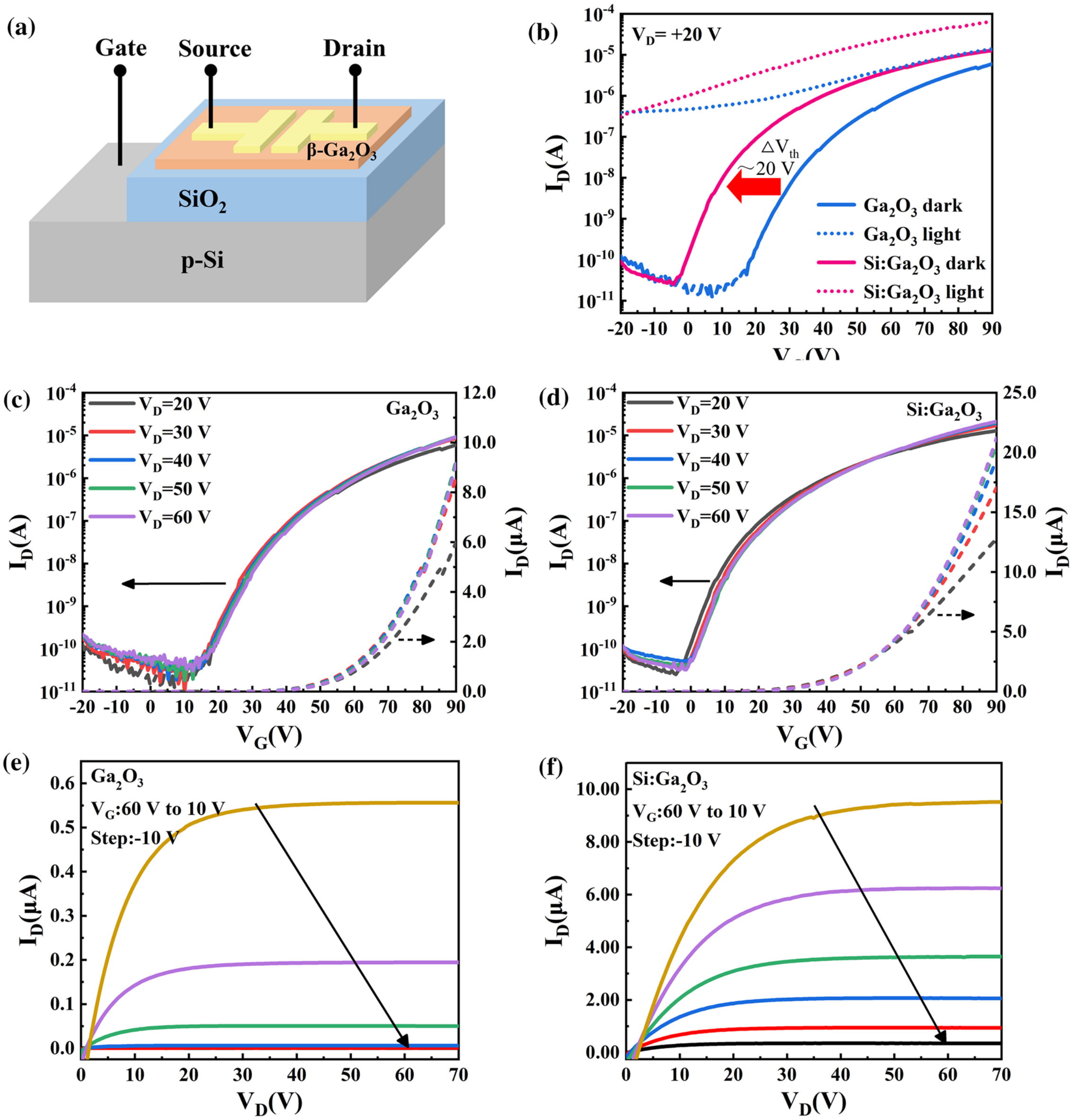

Fig. 3 (a) Schematic structure of the β-Ga_2O_3 TFTs. (b) I_D-V_G transfer curves of pure β-Ga_2O_3 and Si-doped β-Ga_2O_3 TFTs in the dark and under 254-nm light illumination with an intensity of 245.9 μW cm^{-2}. (c, d) I_D-V_G transfer curves of pure β-Ga_2O_3 and Si-doped β-Ga_2O_3 TFTs measured at different V_D in linear and logarithmic scales, respectively. (e, f) I_D-V_D output characteristics with V_G decreasing from 60 V to 10 V with a step voltage of − 10 V in the dark.

Figure 3c and d shows the I_D–V_G transfer curves of pure β-Ga_2O_3 and Si-doped β-Ga_2O_3 TFTs measured at different V_D in linear and logarithmic scales, respectively. From the linear scale, it is clear that I_D grows as V_D increases and, when V_D reaches a certain value, I_D tends to be constant. Figure 3e and f presents the I_D–V_D curves of the two TFTs in the dark, respectively. As we can see, I_D reduces as V_G decreases from 60 V to 20 V, with a step voltage of − 10 V. The comparison shows that the Si-doped sample has a higher value of I_D under different voltages.

To explore the relationship between the photo-response characteristics and light intensity, different light intensities varying from 38.4 μW cm^{-2} to 245.9 μW cm^{-2} have been tested. Figure 4a and b presents the I_D-V_G transfer curves of the pure β-Ga_2O_3 and the Si-doped β-Ga_2O_3 TFTs in the dark and under 254-nm light illumination, respectively, with the intensity varying from 38.4 μW cm^{-2} to 245.9 μW cm^{-2} at $V_D = +20$ V. It is obvious that the photocurrent increases with increasing light intensity, showing a higher I_{light}/I_{dark} ratio. No matter the value of the light intensity, the Si-doped

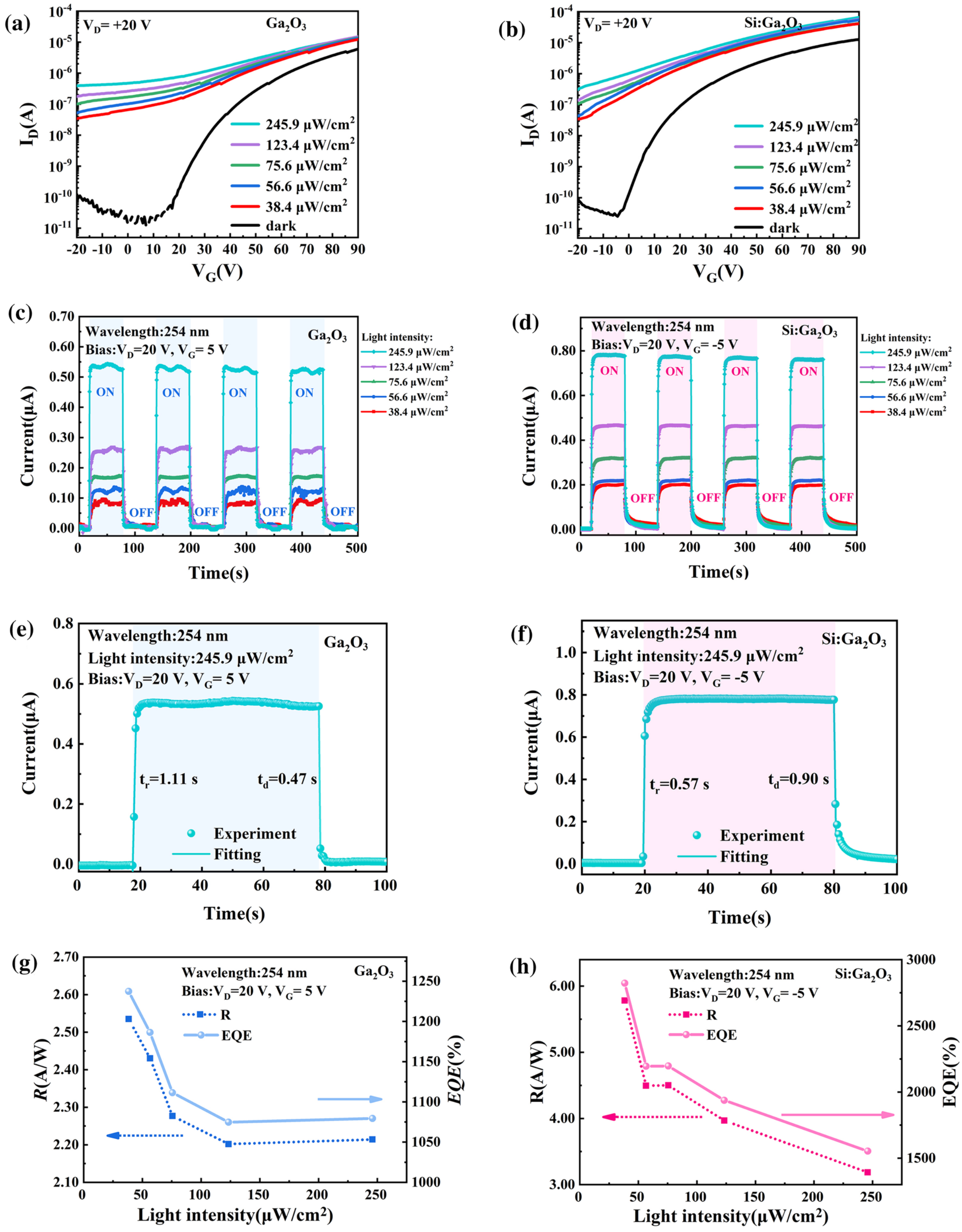

Fig. 4 (a and b) I_D-V_G transfer curves of pure β-Ga_2O_3 and Si-doped Ga_2O_3 TFTs in the dark and under 254 nm light illumination, respectively, with the intensity varying from 38.4 μW cm^{-2} to 245.9 μW cm^{-2}. (c and d) Time-dependent photo-responses of the pure β-Ga_2O_3 and the Si-doped Ga_2O_3 TFTs under 254 nm light with different light intensities, respectively. (e and f) Experimental and fitting curves of the rise and decay process photo-responses, respectively, under 254 nm light with the intensity of 245.9 μW cm^{-2}. (g and h) *R* and EQE as functions, respectively, of light intensity.

sample shows better light sensitivity. The values of the key factors *R*, D^*, and EQE measured under different light intensities are shown in Table SII in Supporting Information.

The I_D–V_D output characteristics with V_G decreasing from 60 V to 10 V, with a step voltage of − 10 V, under different light intensities, are shown in Figure S4 in Supporting

Information. By comparison, the photocurrent of the pure Ga_2O_3 TFT tends to be flat as the V_G increases in the initial stage, while that of the Si-doped sample grows rapidly. Because there are large amounts of defect states in the β-Ga_2O_3 thin films and the Ga_2O_3/SiO_2 interface, most of them serve as carrier-capturing centers. The traps can be populated by photo-excited carriers as V_G increases. Since there are more carriers in the Si-doped sample, the trap-populating process performs faster, and more carriers are involved in the current transmission.[14,32]

The photo-responses of the pure β-Ga_2O_3 and Si-doped Ga_2O_3 TFTs with different light intensities under alternate on and off cycles are shown in Fig. 4c and d, respectively. It can be clearly observed that the photocurrent increases step by step when the light intensity increases gradually. Meanwhile, the Si-doped Ga_2O_3 TFT shows a higher and more stable photocurrent at different light intensities. Figure 4e and f presents the response times of the pure β-Ga_2O_3 and Si-doped Ga_2O_3 TFTs under 254 nm light illumination with the intensity of 245.9 μW cm^{-2}, respectively. The rise time (t_r) and fall time (t_d) are then defined as the times taken by the signal to vary between 10% and 90% of the saturation value. As shown in the photo-response fitting curves, the t_r are 1.1 s and 0.5 s for the TFTs made from pure Ga_2O_3 and Si-doped Ga_2O_3, respectively. And the t_d are 0.4 s and 0.9 s for the TFTs made from Ga_2O_3 without and with Si-doping, respectively. The fast-response component can be attributed to the rapid change of carrier concentration as soon as the light is turned on/off.[33] The t_r for the pure Ga_2O_3 TFT is much higher than that for the Si-doped Ga_2O_3 TFT. The photo-response of a semiconductor is a complex process, including electron–hole generation, trapping, and recombination.[34] The photo-generated carriers may firstly fill the traps and reach their maximum after the traps are saturated, while a lower density of traps is involved in this process for pure β-Ga_2O_3 with better crystalline quality, Si-doping induces more carriers participating in current transfer, which shortens the time to reach the maximum value. The fast decay process indicates weak persistent photoconductivity (PPC), for which the light-induced current persists after the excitation has been removed.[34] The anion vacancies with a metastable state and the presence of surface states may contribute to the PPC behavior.[34–36] According to the XRD curves (see Fig. 1a), the Si-doping method has reduced the crystallinity in the presence of lattice distortion. Dislocation defects can act as recombination centers of non-equilibrium carriers,[37,38] resulting in a longer carrier lifetime in the β-Ga_2O_3 thin film. As shown in Fig. 4g and h, the *R* and EQE, respectively, of both samples decrease with increasing light intensity, which is similar to previous reports.[16,39] The maximum values of *R* and EQE of the Si-doped Ga_2O_3 TFT reach 5.8 A/W and 2.8 × 10^3 , respectively, under 254-nm light illumination with the intensity of 38.4 μW cm^{-2}. The thermal effect-induced carrier scattering and absorption saturation may induce this phenomenon.[39,40]

Figure 5 illustrates the mechanism of the on/off states and photo-responses of semiconductors. An energy band diagram model is proposed to describe the observed transfer characteristics in Fig. 5a–c. Due to the presence of oxygen vacancies both in bulk Ga_2O_3 and the Ga_2O_3 film, a narrow region of depletion with the positively ionized oxygen vacancies appears on the surface of the Ga_2O_3.[41,42] When

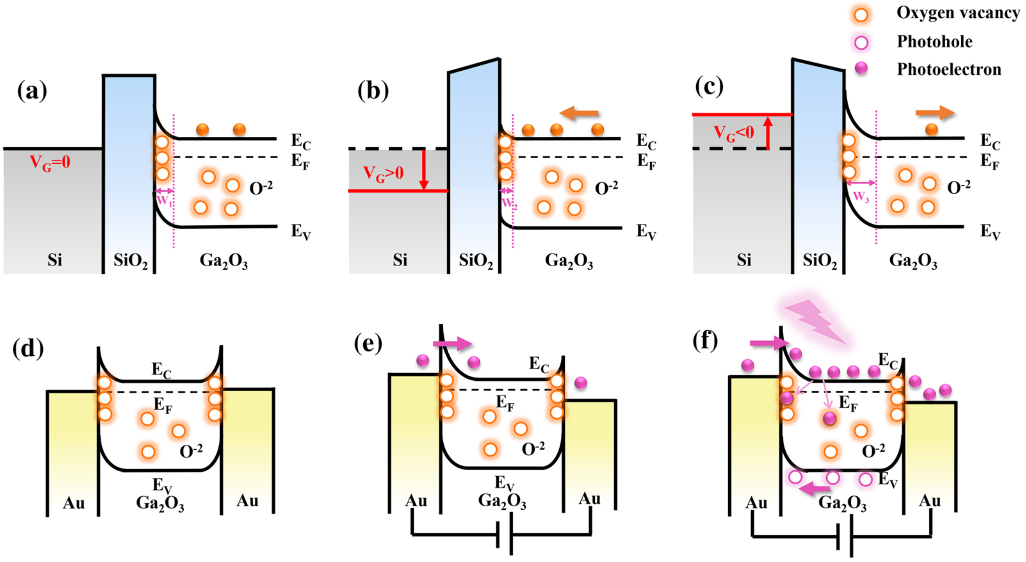

Fig. 5 Schematic energy band diagrams of Ga_2O_3 TFTs. Model of transfer characteristic: (a) $V_G = 0$ V, (b) $V_G > 0$ V, (c) $V_G < 0$ V. Model of photo-conductance process: (d) in the dark without bias, (e) in the dark with bias, (f) under UV illumination with bias.

Table I. Comparison of the key device parameters of our Si-doped Ga_2O_3 solar-blind DUV TFT and other polycrystalline or amorphous Ga_2O_3 thin film photodetectors

Materials	Structures	Growth method	R (A/W)	D^* (Jones)	t_g/t_d (s)	I_{light}/I_{dark}	I_{dark} (A)	Ref.
Amorphous Ga_2O_3:CdO	TFT	Spin-coating	2.17	1.71×10^{12}		1631.15	1.61×10^{-12}	14
Amorphous Ga_2O_3	TFT	RF-magnetron sputtering	4000	2.50×10^{13}	50/> 400			16
Polycrystal β-Ga_2O_3	MSM	RF-magnetron sputtering	96.13		0.032/0.078	> 1000	1.43×10^{-12}	11
Polycrystal β-Ga_2O_3	MSM	Sol-gel method	0.00113		0.1/0.1	78.66	3.28×10^{-9}	33
ZnO/Ga_2O_3 Heterojunction	PN	CVD	> 1000		–	11		9
Polycrystal β-Ga_2O_3	MSM	MOCVD	26.1	1.25×10^{13}	0.48/0.18	10000	3.4×10^{-8}	45
Polycrystal β-Ga_2O_3	MSM	MBE	153		5/10.3	45	7.00×10^{-8}	38
β-Ga_2O_3 Nanosheet	MSM	Mechanical exfoliation	3.3	4.00×10^{12}				31
Polycrystal Si:β-Ga_2O_3	TFT	PLD	3.23	4.41×10^{13}	0.57/0.9	31600	2.51×10^{-11}	This work

using positive V_G bias, the depletion region becomes narrower, which is attributed to conductivity (see Fig. 5b). The applied negative V_G bias expands the depletion width and reduces the effective channel thickness (see Fig. 5c), showing the off state. For the Si-doped Ga_2O_3 TFT, the Si atoms can provide electrons acting as donor, neutralizing the oxygen vacancies at the interface and narrowing the width of the depletion region. The photo-response of a photodetector is a complex process including electron–hole generation, trapping, and recombination.[43,44] Figure 5d–f presents the photoconductance process in the Ga_2O_3 TFTs. Similarly, electrons flow from Ga_2O_3 to metal until both Fermi levels line up (see Fig. 5d). A small number of carriers are able to participate in electron transport when applying positive V_D in the dark (see Fig. 5f). Upon light-on conditions, electron–hole pairs are generated ($hv \rightarrow e^- + h^+$).[41] The photogenerated electrons are trapped in positive charge density in the depletion region.[44] After the recombination between the holes and the oxygen vacancies, the uncombined electrons become the major carriers which contribute to the photocurrent. Upon light-off conditions, oxygen molecules reabsorb onto the surface and current reduces to its original value.

Table I lists several key parameters of our Si-doped Ga_2O_3 solar-blind DUV TFT and other photodetectors based on polycrystalline or amorphous Ga_2O_3 materials with different device structures. The main parameters of our Si-doped Ga_2O_3 solar-blind DUV TFT, such as responsivity, detectivity, and I_{light}/I_{dark} and response times, are better than most other photodetectors based on polycrystalline or amorphous Ga_2O_3 materials. Meanwhile, the TFT structure shows its superiority, resulting in a large I_{light}/I_{dark} ratio and a lower dark current. Furthermore, various methods have been employed to fabricate Ga_2O_3 photodetectors with high performance, but there have been no reports on PLD-prepared TFT-type Ga_2O_3 photodetectors. Our work presents a simple and convenient fabrication process which gives polycrystalline β-Ga_2O_3 TFTs a high potential for the development of photodetectors in the future.

Conclusions

A solar-blind DUV TFT based on polycrystalline β-Ga_2O_3 thin film by PLD has been proposed. The Si-doping method greatly increases carrier transport, although it affects the crystal quality of the thin film. The V_{on} of the Si-doped β-Ga_2O_3 TFT, which works in enhancement mode, was modulated about − 20 V compared to a pure one. The Si-doped Ga_2O_3 TFT displayed excellent transistor characteristics with a high I_D on/off ratio of ~ 10^5, I_{off} of ~ 10^{-11} A at $V_D = + 20$ V. Both β-Ga_2O_3 TFTs showed high sensitivity to 254-nm UV light under different light intensities. An R of 3.23 A/W, an EQE of 1.5×10^3%, a D^* of 4.41×10^{13} Jones and an I_{light}/I_{dark} of ~ 10^3 were achieved at $V_G = - 5$, $V_D = 20$ V for the Si-doped device under 254-nm light illumination with the intensity of 245.9 μW cm^{-2}. Our work provides a new method of Si-doping to improve β-Ga_2O_3 TFTs, which advances the development of DUV TFTs based on Ga_2O_3.

Supplementary Information The online version contains supplementary material available at https://doi.org/10.1007/s11664-022-09599-3.

Acknowledgments This work was supported by National Natural Science Foundation of China (Grant No. 51972283, Grant No. 91833301) and the Key Research and Development Program of Zhejiang Province (2021C01030).

Conflict of interest The authors declare that they have no conflict of interest.

References

1. L. Dong, J. Yu, R. Jia, J. Hu, Y. Zhang, and J. Sun, Self-Powered MSM Deep-Ultraviolet Beta-Ga_2O_3 Photodetector Realized by an Asymmetrical Pair of Schottky Contacts. *Opt. Mater. Express* 9, 1191 (2019).

2. S.J. Pearton, J. Yang, P.H. Cary, F. Ren, J. Kim, M.J. Tadjer, and M.A. Mastro, A Review of Ga_2O_3 Materials, Processing, and Devices. *Appl. Phys. Rev.* 5, 011301 (2018).
3. X. Chen, K. Liu, Z. Zhang, C. Wang, B. Li, H. Zhao, D. Zhao, and D. Shen, Self-Powered Solar-Blind Photodetector with Fast Response Based on Au/beta-Ga_2O_3 Nanowires Array Film Schottky Junction. *ACS Appl. Mater. Interfaces* 8, 4185 (2016).
4. L.-X. Qian, Z.-H. Wu, Y.-Y. Zhang, P.T. Lai, X.-Z. Liu, and Y.-R. Li, Ultrahigh-Responsivity, Rapid-Recovery, Solar-Blind Photodetector Based on Highly Nonstoichiometric Amorphous Gallium Oxide. *ACS Photonics* 4, 2203 (2017).
5. Y.-C. Chen, Y.-J. Lu, C.-N. Lin, Y.-Z. Tian, C.-J. Gao, L. Dong, and C.-X. Shan, Self-Powered Diamond/Beta-Ga_2O_3 Photodetectors for Solar-Blind Imaging. *J. Mater. Chem. C* 6, 5727 (2018).
6. H. Wang, H. Chen, L. Li, Y. Wang, L. Su, W. Bian, B. Li, and X. Fang, High Responsivity and High Rejection Ratio of Self-Powered Solar-Blind Ultraviolet Photodetector Based on PEDOT:PSS/beta-Ga_2O_3 Organic/Inorganic p–n Junction. *J. Phys. Chem. Lett.* 10, 6850 (2019).
7. H.A. Mantooth, M.D. Glover, and P. Shepherd, Wide Bandgap Technologies and Their Implications on Miniaturizing Power Electronic Systems. *IEEE Trans. Emerg. Sel. Topics Power Electron.* 2, 374 (2014).
8. M. Yu, H. Wang, W. Wei, B. Peng, L. Yuan, J. Hu, Y. Zhang, and R. Jia, Analysis of Electronic Structure and Properties of Ga_2O_3/$CuAlO_2$ Heterojunction. *Appl. Surf. Sci.* 568, 150826 (2021).
9. M. Chen, B. Zhao, G. Hu, X. Fang, H. Wang, L. Wang, J. Luo, X. Han, X. Wang, C. Pan, and Z. Wang, Piezo-Phototronic Effect Modulated Deep UV Photodetector Based on ZnO-Ga_2O_3 Heterojuction Microwire. *Adv. Funct. Mater.* 28, 1706379 (2018).
10. B. Zhao, F. Wang, H. Chen, L. Zheng, L. Su, D. Zhao, and X. Fang, An Ultrahigh Responsivity (9.7 mA W-1) Self-Powered Solar-Blind Photodetector Based on Individual ZnO-Ga_2O_3 Heterostructures. *Adv. Funct. Mater.* 27, 1700264 (2017).
11. K. Arora, N. Goel, M. Kumar, and M. Kumar, Ultrahigh Performance of Self-Powered Beta-Ga_2O_3 Thin Film Solar-Blind Photodetector Grown on Cost-Effective Si Substrate Using High-Temperature Seed Layer. *ACS Photonics* 5, 2391 (2018).
12. S. Oh, C.-K. Kim, and J. Kim, High Responsivity Beta-Ga_2O_3 Metal-Semiconductor-Metal Solar-Blind Photodetectors with Ultraviolet Transparent Graphene Electrodes. *ACS Photonics* 5, 1123 (2018).
13. L. Dong, S. Zhou, K. Pu, C. Yang, B. Xin, B. Peng, and W. Liu, Electrical Contacts in Monolayer Ga_2O_3 Field-Effect Tansistors. *Appl. Surf. Sci.* 564, 150386 (2021).
14. X. Xiao, L. Liang, Y. Pei, J. Yu, H. Duan, T. Chang, and H. Cao, Solution-Processed Amorphous Ga_2O_3:CdO TFT-Type Deep-UV Photodetectors. *Appl. Phys. Lett.* 116, 192102 (2020).
15. J. Bae, H.W. Kim, I.H. Kang, and J. Kim, Dual-Field Plated β-Ga_2O_3 Nano-FETs with an Off-State Breakdown Voltage Exceeding 400 V. *J. Mater. Chem. C* 8, 2687 (2020).
16. Y. Qin, S. Long, Q. He, H. Dong, G. Jian, Y. Zhang, X. Hou, P. Tan, Z. Zhang, Y. Lu, C. Shan, J. Wang, W. Hu, H. Lv, Q. Liu, and M. Liu, Amorphous Gallium Oxide-Based Gate-Tunable High-Performance Thin Film Phototransistor for Solar-Blind Imaging. *Adv. Electron. Mater.* 5, 1900389 (2019).
17. Y. Qin, H. Dong, S. Long, Q. He, G. Jian, Y. Zhang, X. Zhou, Y. Yu, X. Hou, P. Tan, Z. Zhang, Q. Liu, H. Lv, and M. Liu, Enhancement-Mode Beta-Ga_2O_3 Metal-Oxide-Semiconductor Field-Effect Solar-Blind Phototransistor with Ultrahigh Detectivity and Photo-to-Dark Current Ratio. *IEEE Electron Device Lett.* 40, 742 (2019).
18. Y. Liu, L. Du, G. Liang, W. Mu, Z. Jia, M. Xu, Q. Xin, X. Tao, and A. Song, Ga_2O_3 Field-Effect-Transistor-Based Solar-Blind Photodetector with Fast Response and High Photo-to-Dark Current Ratio. *IEEE Electron Device Lett.* 39, 1696 (2018).
19. J. Yu, K. Javaid, L. Liang, W. Wu, Y. Liang, A. Song, H. Zhang, W. Shi, T.C. Chang, and H. Cao, High-Performance Visible-Blind Ultraviolet Photodetector Based on IGZO TFT Coupled with p–n Heterojunction. *ACS Appl. Mater. Interfaces* 10, 8102 (2018).
20. H. Altuntas, I. Donmez, C. Ozgit-Akgun, and N. Biyikli, Electrical Characteristics of β-Ga_2O_3 Thin Films Grown by PEALD. *J. Alloys Compd.* 593, 190 (2014).
21. C.X. Xu, H. Liu, X.H. Pan, and Z.Z. Ye, Growth and Characterization of Si-Doped β-Ga_2O_3 Films by Pulsed Laser Deposition. *Optic. Mater.* 108, 110145 (2020).
22. K. Henkel, K. Karavaev, M. Torche, C. Schwiertz, Y. Burkov, and D. Schmeißer, Al-Oxynitride Interfacial Layer Investigations for PrXOYon SiC and Si. *J. Phys. Conf. Ser.* 94, 012004 (2008).
23. M.K. Yadav, A. Mondal, S. Das, S.K. Sharma, and A. Bag, Impact of Annealing Temperature on Band-Alignment of PLD Grown Ga_2O_3/Si (100) Heterointerface. *J. Alloys Compd.* 819, 153052 (2020).
24. M. Fleischer, W. Hanrieder, and H. Meixner, Stability of Semiconducting Gallium Oxide Thin-Films. *Thin Solid Films* 190, 93 (1990).
25. Y. Liu, S.P. Singh, L.M. Kyaw, M.K. Bera, Y.J. Ngoo, H.R. Tan, S. Tripathy, G.Q. Lo, and E.F. Chor, Mechanisms of Ohmic Contact Formation and Carrier Transport of Low Temperature Annealed Hf/Al/Ta on $In_{0.18}Al_{0.82}N$/GaN-on-Si. *ECS J. Solid State Sci. Technol.* 4, P30 (2014).
26. D. Guo, H. Liu, P. Li, Z. Wu, S. Wang, C. Cui, C. Li, and W. Tang, Zero-Power-Consumption Solar-Blind Photodetector Based on Beta-Ga_2O_3/NSTO Heterojunction. *ACS Appl. Mater. Interfaces* 9, 1619 (2017).
27. N. Xu, L.F. Liu, X. Sun, X.Y. Liu, D.D. Han, Y. Wang, R.Q. Han, J.F. Kang, and B. Yu, Characteristics and Mechanism of Conduction/Set Process in TiN/ZnO/Pt Resistance Switching Random-Access Memories. *Appl. Phys. Lett.* 92, 232112 (2008).
28. Y. An, S. Wang, L. Duan, J. Liu, and Z. Wu, Local Mn structure and room temperature ferromagnetism in Mn-doped In_2O_3 films. *Appl. Phys. Lett.* 102, 212411 (2013).
29. Y. Berencen, Y. Xie, M. Wang, S. Prucnal, L. Rebohle, and S. Zhou, Structural and Optical Properties of Pulsed-Laser Deposited Crystalline Beta-Ga_2O_3 Thin Films on Silicon. *Semicond. Sci. Technol.* 34, 035001 (2019).
30. J. Kim, M.J. Tadjer, M.A. Mastro, and J. Kim, Controlling the Threshold Voltage of Beta-Ga_2O_3 Field-Effect Transistors Via Remote Fluorine Plasma Treatment. *J. Mater. Chem. C* 7, 8855 (2019).
31. W. Feng, X. Wang, J. Zhang, L. Wang, W. Zheng, P. Hu, W. Cao, and B. Yang, Synthesis of Two-Dimensional Beta-Ga_2O_3 Nanosheets for High-Performance Solar Blind Photodetectors. *J. Mater. Chem. C* 2, 3254 (2014).
32. M. Fang, W. Zhao, F. Li, D. Zhu, S. Han, W. Xu, W. Liu, P. Cao, M. Fang, and Y. Lu, Fast Response Solar-Blind Photodetector with a Quasi-Zener Tunneling Effect Based on Amorphous In-Doped Ga_2O_3 Thin Films. *Sensors* 20, 129 (2020).
33. H. Shen, Y. Yin, K. Tian, K. Baskaran, L. Duan, X. Zhao, and A. Tiwari, Growth and Characterization of Beta-Ga_2O_3 Thin Films by Sol-Gel Method for Fast-Response Solar-Blind Ultraviolet Photodetectors. *J. Alloys Compd.* 766, 601 (2018).
34. X.Z. Liu, P. Guo, T. Sheng, L.X. Qian, W.L. Zhang, and Y.R. Li, Beta-Ga_2O_3 Thin Films on Sapphire Pre-Seeded by Homo-Self-Templated Buffer Layer for Solar-Blind UV Photodetector. *Opt. Mater.* 51, 203 (2016).
35. P. Sen, M. Balasubrahmaniyam, D. Kar, and S. Kasiviswanathan, Size-Dependent Persistent Photocurrent and Its Origin in DC Sputtered Indium Oxide Films Under UV and Sub-Band Gap Illuminations. *J. Appl. Phys.* 121, 185303 (2017).
36. P. Sen, D. Kar, R. Laha, M. Balasubrahmaniyam, and S. Kasiviswanathan, Hot Electron Mediated Enhancement in the Decay

Rates of Persistent Photocurrent in Gold Nanoparticles Embedded Indium Oxide Films. *Appl. Phys. Lett.* 114, 211103 (2019).

37. Z. Alaie, S.M. Nejad, and M.H. Yousefi, Recent Advances in Ultraviolet Photodetectors. *Mater. Sci. Semicond. Process.* 29, 16 (2015).
38. L.X. Qian, Y. Wang, Z.H. Wu, T. Sheng, and X.Z. Liu, Beta-Ga_2O_3 Solar-Blind Deep-Ultraviolet Photodetector Based on Annealed Sapphire Substrate. *Vacuum* 140, 106 (2017).
39. W. Kong, G. Wu, K. Wang, T. Zhang, Y. Zou, D. Wang, and L. Luo, Graphene-Beta-Ga_2O_3 Heterojunction for Highly Sensitive Deep UV Photodetector Application. *Adv. Mater.* 28, 10725 (2016).
40. W.J. Yu, Y. Liu, H. Zhou, A. Yin, Z. Li, Y. Huang, and X. Duan, Highly Efficient Gate-Tunable Photocurrent Generation in Vertical Heterostructures of Layered Materials. *Nat. Nanotechnol.* 8, 952 (2013).
41. L. Li, E. Auer, M. Liao, X. Fang, T. Zhai, U.K. Gautam, A. Lugstein, Y. Koide, Y. Bando, and D. Golberg, Deep-Ultraviolet Solar-Blind Photoconductivity of Individual Gallium Oxide Nanobelts. *Nanoscale* 3, 1120 (2011).
42. J. Ma, and G. Yoo, Surface depletion effect on negative bias stress instability of beta-Ga_2O_3 (100) nanomembrane FETs. *Jpn. J. Appl. Phys.* 58, SBBD01 (2019).
43. D. Guo, J. Wang, C. Cui, P. Li, X. Zhong, F. Wang, S. Yuan, K. Zhang, and Y. Zhou, ZnO@TiO_2 Core–Shell Nanorod Arrays with Enhanced Photoelectrochemical Performance. *Sol. Energy* 95, 237 (2013).
44. D.Y. Guo, Z.P. Wu, Y.H. An, X.C. Guo, X.L. Chu, C.L. Sun, L.H. Li, P.G. Li, and W.H. Tang, Oxygen Vacancy Tuned Ohmic–Schottky Conversion for Enhanced Performance in Beta-Ga_2O_3 Solar-Blind Ultraviolet Photodetectors. *Appl. Phys. Lett.* 105, 023507 (2014).
45. D. Zhang, W. Zheng, R.C. Lin, T.T. Li, Z.J. Zhang, and F. Huang, High Quality Beta-Ga_2O_3 Film Grown with N_2O for High Sensitivity Solar-Blind-Ultraviolet Photodetector with Fast Response Speed. *J. Alloys Compd.* 735, 150 (2018).

Publisher's Note Springer Nature remains neutral with regard to jurisdictional claims in published maps and institutional affiliations.